ingegneria sismica
International Journal of Earthquake Engineering
Anno XLIII - Num. 3 - 2026

Thermal stress analysis and simulation of high-performance building materials in extreme climatic environments

Jiao Chen[1], *Zhi Zhuang*[2,*] *and Jiankun Liang*[1]

[1] School of Architectural Engineering, Kaili University, Qiandongnan 556011, Guizhou, China

[2] College of Architecture and Urban Planning, Tongji University, Shanghai 200000, China

SUMMARY: *Traditional concrete materials will cause more or less damage to the ecological environment, whether from the production or application stage, while high-performance building materials can well avoid this risk of environmental damage. This paper refers to the relevant information, selects the raw materials studied in this paper, and prepares the high-performance building materials under the guidance of the preparation method and process. ABAQUS finite simulation analysis software was selected as the data analysis tool for this study, and the tool was used to investigate the thermal stress changes of high-performance building materials in extreme climatic environments. Under the action of extreme climate environment, it is found that the fiber volume content and the thermal stress of high-performance building materials have a monotonically increasing trend, and its value rises from 2.452MPa to 15.753MPa, which is a good presentation of the change rule of thermal stress in high-performance buildings, and it provides a reference for the research and development and innovation of building materials.*

KEYWORDS: *simulation analysis software; high-performance building materials; extreme climate environment; thermal stress*

1 Introduction

With the progress of science and technology and the development of society, people have higher and higher requirements for building materials. As a new type of building materials, high-performance building materials have excellent mechanical properties, durability, environmental protection and other characteristics [1, 2]. Before the emergence of high-performance building materials, traditional building materials have been the main materials in the construction field. However, traditional building materials have certain limitations in terms of strength, durability, and energy efficiency [3-5]. For example, concrete has certain bottlenecks in terms of compressive strength and durability, which cannot meet the needs of large-span buildings and ultra-high-rise buildings [6, 7]. Steel also has certain problems in terms of corrosion resistance and durability, especially in the application of high temperature and strong corrosive environments with greater limitations [8, 9]. Therefore, the limitations of traditional building materials have given rise to the emergence and development of high-performance building materials. High-performance building materials can improve the quality and safety of buildings, reduce construction costs, reduce energy consumption, and favor environmental protection [10-

*1008560@mymail.sutd.edu.sg
https://doi.org/10.65102/is20261060
Published: 10 June, 2026

12]. In this context, analyzing thermal stresses and simulation calculations in extreme climatic environments has become a current research hotspot in the construction industry.

Thermal stress is the stress inside the material due to temperature change [13]. When a material is subjected to temperature changes, internal stresses are generated due to the inconsistent temperatures in different parts [14]. The magnitude of thermal stresses is related to the coefficient of thermal expansion of the material, which is the proportionality coefficient of the change in length or volume of a material per unit change in temperature, and the study of thermal stresses is crucial for the design and safety assessment of building structures [15-18]. In extreme climatic environments, temperature changes cause expansion and contraction of building materials, which in turn generate stresses and deformations [19, 20]. By studying the coefficient of thermal expansion of high-performance building materials and the effect of temperature change on the structure, the building structure can be rationally designed to ensure its safety performance under temperature change [21, 22].

Literature [23] and literature [24] describe Ultra High Performance Concrete (UHPC) and its characteristics such as ease of use, self-casting and self-consolidation, emphasizing the fact that UHPC can be widely used as a sustainable, long-term solution for civil engineering buildings and networks. Literature [25] describes the application of high performance building materials to improve the sustainability and durability of infrastructure, elaborating that the use of fibers to develop highly ductile fiber-reinforced cementitious composites has become a national consensus, and that silica fume, among others, has emerged as nanomaterials to improve the mechanical properties and microstructure of concrete. Literature [26] introduced UHPC, and the comparison between UHPC and ordinary concrete with superior mechanical properties, excellent seismic performance and other characteristics, and analyzed the research and application of UHPC in bridge engineering, outlining the practical application of UHPC in bridge load-bearing members, bridge joints and other aspects. Literature [27] describes that UHPC should have excellent mechanical properties and durability, and provides a systematic review of the properties of UHPC and its application in bridge engineering, indicating the application of various bridge components, such as piers and girders. The above study describes high-performance construction materials and their characteristics and applications, which are mainly characterized by seismic resistance, self-tightness, and mechanical properties, and are widely used in buildings and bridges.

Literature [28], in order to understand the performance of buildings in extreme heat and the potential stress on people, evaluated the indoor air temperature changes when air conditioning is not available by modeling a building prototype, pointing out that measures should be taken in order to counteract the vulnerability of infrastructures and to provide thermal refuge for the inhabitants. Literature [29] numerically simulated, the temperature rise and stress during hydration of UHPC using finite element based numerical modeling, showing that a severe thermal gradient occurs within the UHPC members, which results in high thermal stresses and leads to surface cracking of the concrete structure, pointing out the influencing factors and countermeasures. Literature [30] aimed to establish the thermal expansion-temperature curves of UHPC and HSC over the temperature range of -76 to 140 degrees F. Based on the considered temperature range, it was verified that the coefficient of thermal expansion of UHPC is constant, and the results of the study are expected to be used for the calculation of the thermal stresses between the UHPC and HSC composite structures in bridge design/analysis. Literature [31] evaluated the behavior of constrained high-performance concrete in response to extreme heating associated with fire and calculated the thermal stresses based on the thin-walled cylinder model theory, which was verified to be suitable for the determination of the spalling initiation point and the depth of spalling by proposing a spalling damage model based on the

tensile strain damage model. Literature [32] explored the potential application of phase change materials (PCMs) integrated into buildings to reduce the risk of heat stress during extreme heat waves, demonstrating that PCM retrofits can be effective in reducing the risk of indoor heat stress, providing significant benefits in terms of improving occupant health and comfort, and reducing indoor heat stress. The above study then examines the thermal stress of high-performance building materials in extreme heat environments, indicating the factors that influence it and its application prospects.

Based on relevant information and References, this paper determines the raw materials for this research, and accomplishes the task of preparing specimens of high-performance building materials based on the preparation methods and processes. In order to make the results of this research clear, intuitive and three-dimensional, it is proposed to use ABAQU finite element simulation and analysis software as the main analytical tool, and on the basis of the theoretical knowledge of thermodynamics, to derive the thermal stress test and calculation formula of high-performance building materials. Under the joint action of the simulation and analysis software and the thermal stress calculation formula, numerical simulation and analysis of the thermal stress of high-performance building materials in extreme climatic environments are carried out, aiming at revealing the thermal stress changes of high-performance building materials in extreme climatic environments.

2 Raw Materials and Preparation of High Performance Building Materials

2.1 Raw materials

2.1.1 Cementing materials

The cement used for the experiment was P·W-I52.5 WPC, which was produced by a limited company, limestone powder was limestone powder produced by a new material limited company, metakaolin was Jiangsu calcined metakaolin, and silica fume was white silica fume produced by Hengyuan New Material Co. The main chemical composition, whiteness and loss on burning of the cementitious materials are shown in Table 1, the particle size distribution is shown in Fig. 1, and the main physical phase is shown in Fig. 2.

Table 1: Chemical composition (wt%) and whiteness (%) of experimental materials

Material	CaO	SiO_2	Al_2O_2	Fe_2O_3	MgO	Na_2O	K_2O	P_2O_5	SO_3	Whiteness	LOI
WPC	67.84	17.76	2.253	0.271	4.531	0.309	0.696	0.013	4.424	87.75	2.472
SF	0.284	90.92	0.472	0.394	0.328	0.113	0.044	1.192	0.962	91.99	0.133
MK	0.476	94.81	0.887	0.052	0.277	0.046	0.125	0.016	0.243	95.53	0.058
LP	98.68	0.212	0.036	0.028	0.283	-	-	0.032	0.025	96.76	7.083

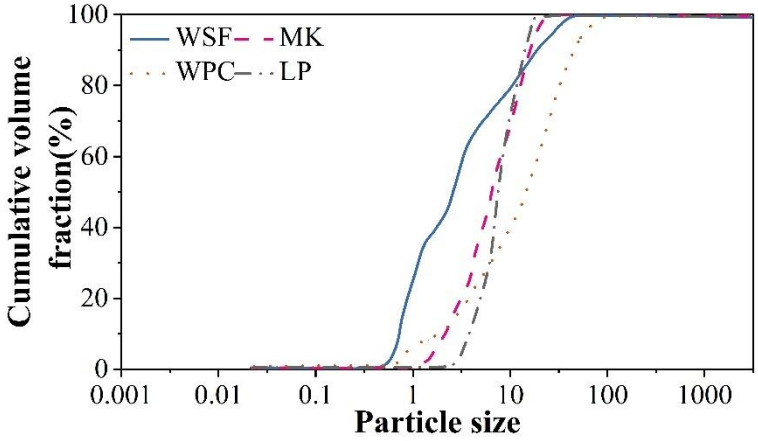

Figure 1: Particle size accumulation curve of cementitious material

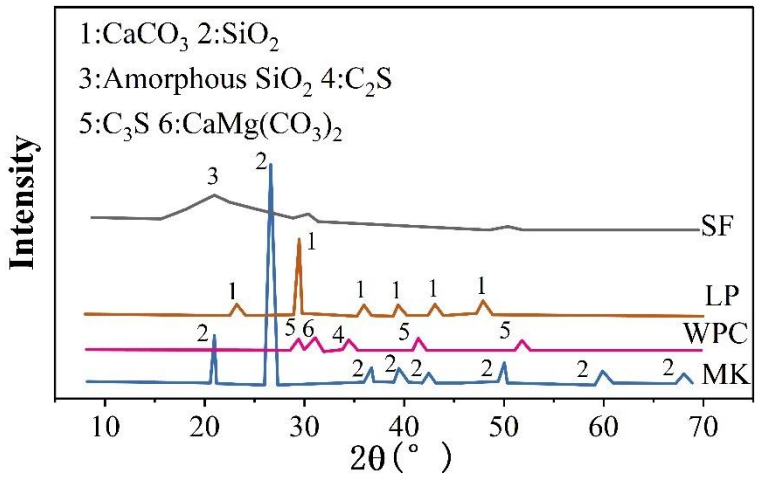

Figure 2: XRD patterns of binders

2.1.2 Aggregates

The fine aggregate used in the experiment was natural river sand, and the sieving curve of the sand measured according to the standard of GBT 14684-2011 Sand for Construction is shown in Fig. 3, and the river sand used was Class II sand. The river sand used is class II sand with fineness modulus of 2.58 and apparent density of 2.59g/cm³.

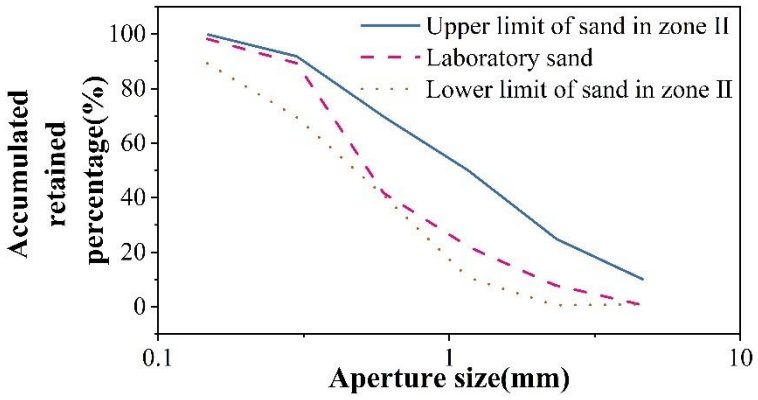

Figure 3: Screening curve of sand

2.1.3 Steel fibers

The experiments were carried out using copper-plated straight steel fibers (SSF) of the dramix type manufactured by Bekaert, and copper-plated steel fibers (HSF) of the RS60 end-hook type manufactured by Shanghai Zhenqiang Fiber Co. Their physical properties are shown in Table 2.

Table 2: Properties and morphology of SSF and HSF used in experiment

Type	Length (L) /mm	Equivalent diameter (D) /mm	L/D radio	Tensile strength/MPa
SSF	11	0.213	80	2780
HSF	11	0.213	80	2780

2.1.4 Titanium dioxide nanoparticles

The titanium dioxide nanopowder used in the experiments was a commercial titanium dioxide nanopowder produced by Aladdin (its crystal type is anatase) with a particle size of 30 nm.

2.1.5 Cellulose fibers

The cellulose fiber used in the experiment was UF500 cellulose fiber (CF) produced by Shanghai New Materials Co. and its basic physical properties are shown in Table 3.

Table 3: Physical properties of cellulose fibers

Ultimate compressive strength/MPa	Elastic Modulus/GPa	Ultimate elongation/%	Equivalent diameter/um	Monofilament length/mm	Density g/cm³
500~1000	25~40	3.43	10~20	2~6	1.03

2.1.6 Water reducing agents

The water reducing agent used in the experiment was MELMENT 4930F polycarboxylic acid water reducing agent produced by BASF, Germany, and the water reducing rate was more than 30%.

2.2 Preparation of high-performance building materials

2.2.1 Preparation methods

In the process of preparing high-performance building materials, the high-temperature reaction system method is one of the more traditional specific methods, and it is also the most economical, efficient and stable of many specific methods. Generally speaking, the reaction system reaction occurs when the general situation is how to operate, are liquid white powder as raw materials. Weighing the raw materials used in a certain proportion to achieve the required impurity content, and add a certain amount of from the side to assist in the full mixing and crushing of alumina, and then under certain conditions (ambient temperature, tension atmosphere, etc.) flame combustion. With reference to the combination of quantum dots technology of physical and chemical metrology standard ratios, the formula ratios are very accurate, under high temperature conditions, in the non-destructive and tense atmosphere or ambient reductant placed in a box-type resistance furnace and the atmosphere, the flame burns at 500 ℃ ~ 1600 ℃ 1h-3h. High temperature solid-phase method on the temperature of the reaction process will have how to start the discussion. In addition, the preparation of high-performance building materials, combustion method, precipitation method, sol-gel method and

so on.

2.2.2 Preparation process

The process of preparation of high performance building materials is shown in Fig. 4, which is taken in this section to prepare high performance building materials using high temperature solid phase method. High-temperature solid-phase synthesis refers to the gradual formation of a large number of complex oxides. In the early stage of the reaction, the surface of the raw material will be in contact with the interface, and then gradually diffuse into the interior of the raw material. Therefore, the raw materials are ground as evenly as possible so that they can fully react.

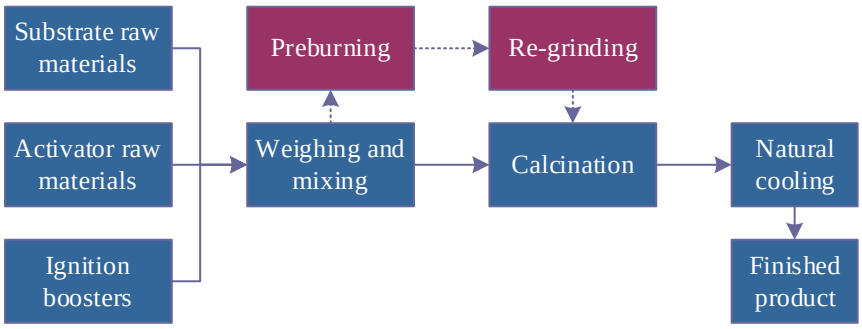

Figure 4: High performance building material preparation process

3 Exploration of thermal stress in extreme climatic environments

3.1 Extreme climatic environments

The IPCC Fourth Assessment Report states that under different future greenhouse gas emission scenarios, the frequency of heat wave events will increase in global land areas, while the number of cold and frost days will decrease, the frequency of extreme precipitation events, such as heavy rainfall, will increase, precipitation will increase, the extent of droughts will expand, and the number of strong typhoons will increase. Extreme climate change is consistent with the state of global change, with changes in the frequency and intensity of extreme weather events since 1951.

3.1.1 Extreme temperature variations

Both the average maximum and minimum temperatures show an increasing trend, and the increasing trend of the minimum temperature is more significant. In the last 50 years (1980-2018), the annual average maximum and minimum temperature increase rates were 0.18°C/10a and 0.54°C/10a, respectively, and the increase rate of the minimum temperature was almost three times of the increase rate of the minimum temperature.

3.1.2 Extreme precipitation variability

Over the past 50 years, annual precipitation has generally tended to decrease, with less light rainfall but more heavy rainfall and extreme precipitation. This trend is particularly evident after the 1990s. The number of precipitation days has decreased in most areas, and the intensity of heavy rainfall levels and extreme precipitation has increased. The frequency and intensity of

precipitation directly affect the level and severity of flooding.

3.1.3 Changes in the incidence of drought

With global warming, the area of arid regions has expanded in recent years, and some humid and semi-humid areas have been transformed into arid zones. The frequency of droughts has increased, with the frequency of droughts in parts of Northeast, South and North China increasing by 30-50%. The extent of drought has increased, with 23 provinces and regions experiencing severe drought and 14 provinces and regions experiencing extreme drought during the period 1980-2007, an increase of five and nine provinces and regions respectively over the period 1949-1979.

3.2 Simulation and analysis software

3.2.1 Finite element simulation analysis

Finite element simulation analysis (FEM) is a continuous complex physical problems simplified into a finite number of units and unit nodes to solve mathematical problems, with high efficiency, wide range of applications and strong reliability. Its basic idea is to discretize the complex solution area into a finite number of small cells, and set a finite number of nodes on the unit, the solution area is simplified into a small unit assembly connected through the nodes, these nodes constitute a grid to discretize the solution domain, a complex problem into a number of simple problem solving. Finite element simulation and analysis of complex physical problems into algebraic problems, the unit of algebraic equations for interpolation and do the domain and boundary integral solution, you can find the original problem of the approximate numerical solution. At the same time, in the case of mathematical conditions are met, the higher the degree of discretization, the higher the accuracy of the solution, the larger the amount of computation, the lower the computational efficiency.

Finite element simulation analysis is divided into three stages: pre-processing stage, operation and solution stage and post-processing stage. The pre-processing stage includes defining the physical properties of the model, selecting the solution method, setting the loads and interactions, meshing the model and finally generating the finite element input file, and mesh delineation is the basic problem of finite element calculation. The operation and solution stage includes three steps: derivation of formula equations, discrete equations and solution equations, and the common solution methods include implicit solution and explicit solution, which are realized in the analysis software, and the time for operating a solution process varies, depending on the complexity of the model and the configuration of the computer. The post-processing stage is to analyze and characterize the results of the operation, and users can extract and view the operation data through the simulation module of the finite element related software.

3.2.2 ABAQUS finite element analysis software

ABAQUS is an engineering analysis finite element simulation software developed by HKS, which has good solution capabilities for simple linear analysis and complex nonlinear problems [33]. Especially for large complex models and highly nonlinear problems, it is possible to perform single-part analyses and model-system level studies, e.g., to analyze complex solid mechanics and structural mechanics problems. In real physical problems, there are nonlinear problems between external loads and internal system response, and ABAQUS is known as “the most advanced large-scale general-purpose nonlinear finite element simulation and analysis software in the world”, which has a good solution for such problems.

3.3 Heat transfer performance testing of building materials

In this subsection, the heat transfer properties of high-performance building materials are tested in the presence of extreme climates and simulation and analysis software. Heat transfer performance testing indicates the inherent law of the energy transfer process of building materials, where heat flows spontaneously from a high temperature object to a low temperature object as long as a temperature difference exists. In nature, the heat transfer process is formed by a combination of three basic heat transfer methods: thermal conductivity, thermal convection and thermal radiation, which occur simultaneously in most extreme climatic environments.

3.3.1 Basic modes of heat transfer from building materials

(1) Thermal conductivity

Thermal conductivity, also known as thermal conduction, mainly occurs when there is no relative displacement of parts within an object or when different objects are in direct contact, and the transfer of heat is realized through the thermal movement of microscopic particles such as molecules and atoms [34]. The process of heat conduction strictly follows Fourier's law, and the heat flow through an arbitrary cross-section during heat conduction can be expressed as:

$$Q = -\lambda \frac{\partial T}{\partial n} \tag{1}$$

In the formula:

Q - heat flow density, the meaning of which is the heat flow transferred through the unit area per unit time, (W / m^2).

λ - coefficient of thermal conductivity, reacting to the high or low thermal conductivity of the material or the strength of thermal conductivity efficiency, $W / (m \cdot K)$.

n - direction normal to the cross-section.

T - temperature, °C.

$\partial T / \partial n$ - rate of change of temperature in the normal direction.

(2) Thermal convection

The process of heat transfer from one place to another through the movement of a fluid is called thermal convection [35]. However, in heat transfer engineering, we are often faced with not only pure heat convection, but more fluid and solid wall in direct contact with the heat exchange process, this process is called “convective heat transfer”. In nature, convective heat transfer is mainly divided into two categories: natural convection and forced convection. The classical formula for calculating convective heat transfer was proposed by Isaac Newton. That is:

$$Q = h(t_w - t_f) = h\Delta t \tag{2}$$

or

$$\Phi = h(t_w - t_f)A = h\Delta t \tag{3}$$

In the formula:

h - convective heat transfer surface heat transfer coefficient, the significance of which refers to the unit area, the fluid with the wall surface of the unit temperature difference between the heat transferred in a unit of time, $W / (m^2 \cdot K)$.

t_w - solid wall surface temperature, ℃.

t_f - fluid temperature, ℃.

Δt - temperature difference between wall surface and fluid, ℃.

A - area of heat transfer surface, m^2.

Φ - convective heat transfer capacity, W.

(3) Thermal radiation

Thermal radiation, as an inherent property of all types of matter in nature, is mainly used to realize heat transfer through visible and invisible rays emitted outward from the surface of an object [36]. When it comes to an ideal thermally radiating surface, the process of radiation follows the well-known Stephen Boltzmann's law, viz:

$$\phi = \vartheta_b T^4 A(W) \tag{4}$$

Eq:

θ_b - Stephen Boltzmann constant, $W/(m^2 \cdot K^4)$.

T - thermodynamic temperature, K.

$A(W)$ - area of an object subject to radiation, m^2.

3.3.2 Differential equations for thermal conductivity of building materials and their solution conditions

(1) Differential equation of thermal conductivity

Based on the law of conservation of energy and Fourier's law of thermal conductivity, a three-dimensional unsteady differential thermal conductivity equation is constructed. This equation can reveal how the temperature of an object varies with time and space. In Cartesian spatial Cartesian coordinate system, this equation is expressed in concrete form:

$$\rho c \frac{\partial t}{\partial \tau} = \frac{\partial}{\partial x}\left(\lambda \frac{\partial t}{\partial x}\right) + \frac{\partial}{\partial y}\left(\lambda \frac{\partial t}{\partial y}\right) + \frac{\partial}{\partial z}\left(\lambda \frac{\partial t}{\partial z}\right) + \dot{\varphi} \tag{5}$$

Eq:

ρ - density of the object material, kg/m^3.

c - specific heat capacity of the object material, $J/(kg \cdot K)$.

t - ambient temperature, ℃.

τ - time interval, s.

λ - thermal conductivity of the object, $W/(m \cdot K)$.

x, y, z - dimensions of the object (length, width and height), m.

$\dot{\varphi}$ - heat energy generated per unit volume per unit time, W/m^3.

When $\dot{\varphi}$ is 0, i.e., no heat source is generated in the object, and the thermal conductivity of the object is a fixed constant, Eq. (5) can be simplified to the following expression:

$$\frac{\partial^2 t}{\partial x^2} + \frac{\partial^2 t}{\partial y^2} + \frac{\partial^2 t}{\partial z^2} = 0 \tag{6}$$

(2) Fixed solution conditions

Examined from a mathematical point of view, solving the differential equations for thermal

conductivity does lead to a generic solution of the equation. However, for a specific thermal conductivity process, it is not enough to obtain the generic solution. It is also necessary to find that unique solution that satisfies both the differential equation for thermal conductivity and the specific additional conditions for that process. These specific additional conditions, which are used to further limit and specify the range of the solution, are called fixed solution conditions. In short, the solution condition is the key additional information that helps to find the unique solution for a particular thermal conductivity process. Fixed solution conditions are generally characterized by the following four items:

1) Geometric conditions

Describe the geometric configuration and volume scale of the objects involved in the thermal conductivity process.

2) Physical conditions

Clarify the properties of the objects involved in the thermal conductivity process on the physical plane, especially with respect to the specific values of thermal conductivity, specific heat capacity, and density, and indicate whether these values change due to fluctuations in temperature.

3) Time conditions

Indicate the different manifestations of thermal conductivity processes in time. In this case, the steady state thermal conductivity process does not change with time and there is no need to consider the time condition. However, unsteady thermal conductivity processes require special attention to the temperature distribution at their starting moment.

4) Boundary conditions

The expression of boundary conditions can usually be categorized into three types:

a) The value of the temperature at the boundary of the object is known at any point in time, i.e.:

$$t\big|_s = f_{1\tau} \tag{7}$$

b) The value of the heat flow density on the boundary surface of the object at any instant is known and is expressed in the form:

$$q\big|_s = f_{2\tau} \tag{8}$$

c) The known fluid temperature t_f around the boundary surface and the surface heat transfer coefficient h between the boundary surface and the fluid can be expressed as:

$$-\lambda \left.\frac{\partial t}{\partial n}\right|_s = h(t\big|_s - t_f) \tag{9}$$

3.3.3 Thermal stresses in construction materials

To calculate the temperature stress of an object based on the known temperature field within the elastomer, the elastomer is decomposed as a connection of numerous tiny ortho-hexahedra (microelements), with the temperature change of each microelement denoted as T. When the temperature of each microelement changes without constraint, the microelement will experience a linear strain αT, α being the coefficient of linear expansion of the object. In the usual thermal stress problem it is assumed that α is a constant, due to the external constraints and mutual constraints between the parts, the free deformation is only an ideal case, so the elastomer deformation can be expressed as:

$$\begin{cases} \varepsilon_x = \dfrac{1}{E}[\sigma_x - \mu(\sigma_y + \sigma_z)] + \alpha T \\ \varepsilon_y = \dfrac{1}{E}[\sigma_y - \mu(\sigma_x + \sigma_z)] + \alpha T \\ \varepsilon_z = \dfrac{1}{E}[\sigma_z - \mu(\sigma_y + \sigma_x)] + \alpha T \end{cases} \tag{10}$$

$$\begin{cases} \gamma_{xy} = \dfrac{2(1+\mu)}{E}\tau_{xy} \\ \gamma_{zx} = \dfrac{2(1+\mu)}{E}\tau_{zx} \\ \gamma_{yz} = \dfrac{2(1+\mu)}{E}\tau_{yz} \end{cases} \tag{11}$$

Assuming that the temperature does not change with the change in the direction of the object Z and there is no body force and surface force, equation (9) can be simplified, the simplified equation can be obtained by solving the strain and temperature change expressed stress expression, and then substituting differential equations for the collation of tanks according to the displacement and temperature to solve the stress expression is as follows:

$$\begin{cases} \sigma_x = \dfrac{E}{1-\mu^2}\left(\dfrac{\partial u}{\partial x} + \mu\dfrac{\partial v}{\partial y}\right) - \dfrac{E\alpha T}{1-\mu} \\ \sigma_y = \dfrac{E}{1-\mu^2}\left(\dfrac{\partial v}{\partial y} + \mu\dfrac{\partial u}{\partial x}\right) - \dfrac{E\alpha T}{1-\mu} \\ \tau_{xy} = \dfrac{E}{2(1+\mu)}\left(\dfrac{\partial v}{\partial x} + \dfrac{\partial u}{\partial y}\right) \end{cases} \tag{12}$$

where: u denotes the amount of deformation occurring in the length direction of the material, $m.\ v$ represents the amount of deformation occurring in the width direction of the material, $m.\ \mu$ represents the Poisson's ratio of the object.

High-performance building materials are favored as special plates for engineering projects because of their good physical properties and usability. And such materials belong to the category of plastic materials, its common failure mode is usually yield failure, so according to the fourth strength theory, using von Mises stress criterion as the material structure strength failure determination index, the fourth strength theory formula is as follows:

$$\sigma = \sqrt{\frac{1}{2}\left[(\sigma_1 - \sigma_2)^2 + (\sigma_2 - \sigma_3)^2 + (\sigma_3 - \sigma_1)^2\right]} \le [\sigma] \tag{13}$$

4 Exploration of thermal stresses in building materials

4.1 Numerical simulation experiment setup

4.1.1 Operational steps

A refined numerical model is used to analyze and validate the strain changes of high-performance building materials under extreme climatic environments. Material properties, temperature field changes, moisture migration and phase change, structural geometry and boundary conditions, mesh refinement and numerical stability are all taken into account to more accurately simulate and analyze the strain change behavior of high-performance building materials under extreme climatic environments.

4.1.2 Computational modeling of buildings

The computational model was developed in 2 steps using sequential coupled thermal stress analysis. Specifically as follows:

(1) Establish the heat transfer model, which includes 3 components: masonry wall, insulation board and mortar layer, and all three are modeled with solid units.

(2) For thermal stress analysis, the type of mesh adopts the three-dimensional stress type. The size of meshing is the same as the grid size of heat conduction analysis. The temperature stress is generated on the model surface by the temperature field action.

4.1.3 Boundary condition settings

The surface of the mortar layer of the building material is given a temperature condition of -25~25°C, and the ambient temperature of the building material is 10°C. The initial temperature of the finite element model of the building material structure can be set to 10°C. In addition to the outer surface of the mortar layer of the building material structure, the rest of the surfaces are set as adiabatic boundary condition pieces to ensure that the temperature only enters the interior of the structure from the surface of the material.

4.2 Temperature change rule analysis

Figure 5 shows a schematic diagram of the temperature change of the mortar layer of the building material structure under the action of extreme environment. From Fig. 5(a), it can be seen that the mortar layer on the surface of the building material structure is in direct contact with the external environment, and the temperature change is more obvious than the remaining 2 layers. From Fig. 5 (b), it can be seen that when the temperature cycle reaches 43°C, the outer surface of the mortar rapidly reaches 43°C, and the temperature distribution is increasing from inside to outside. From Fig. 5 (c), it can be seen that the temperature of the inside of the cement mortar is cyclic, the lowest temperature is close to -43 ℃, the highest temperature peak is close to 43 ℃, the length of the cycle is about 8h, which is in line with the change rule of the temperature of the material in the test environment.

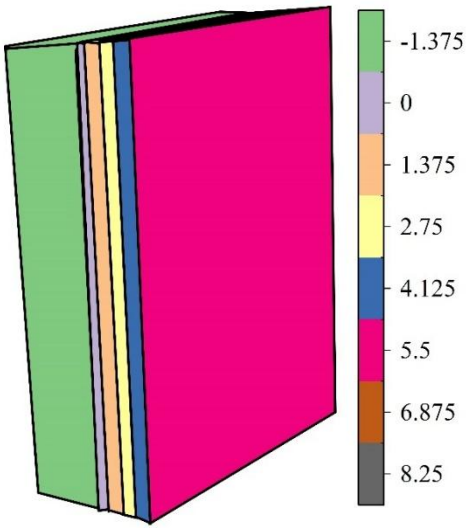

(a)Temperature drop gradient

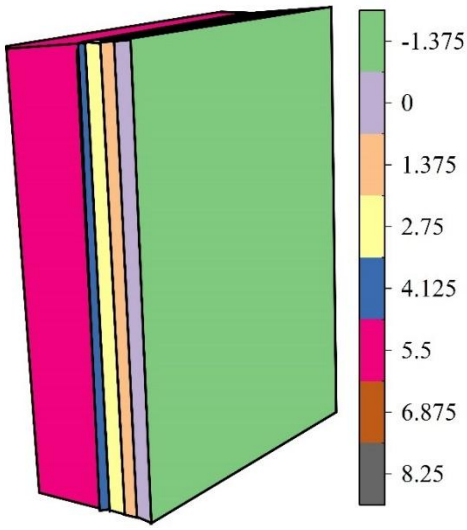

(b)Temperature rise gradient

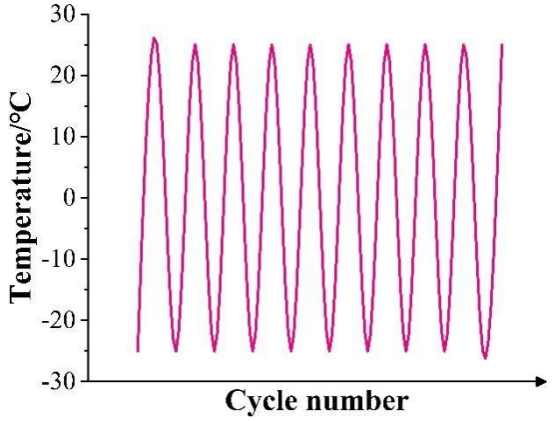

(c) Simulate the temperature change curve

Figure 5: Temperature variation diagram

4.3 Strain pattern analysis

The extreme environmental conditions are simulated by setting specific ambient temperatures and boundary conditions, and the strain curves of the cement mortar layer, the polypropylene fiber mortar layer, and the polymer mortar layer under the effect of the environment are finally obtained (see Fig. 6), as well as the strain cloud diagram of the structural wall of the building material (see Fig. 7). From Fig. 6(b) and Fig. 6(c), it can be seen that the maximum strain values of the numerically simulated polypropylene fiber mortar layer and the polymer mortar layer mortar are 3.0×10^5 and 4.0×10^5, respectively. The mortar layer is the part with the largest strain in the whole material. As shown in Fig. 6(a), the maximum simulated strain value of the cement mortar layer is 30×10^5, and the simulated strain curve is consistent with the trend of the test curve. In Fig. 7, when the strain value of the cement mortar layer increases to 1.2e-04, the crack stops developing and the strain no longer increases, and the other two are the same. The finite element simulation results have a small error with the test results, which are basically consistent with the results of the test, and well reveal the internal and external strain laws of high-performance building materials in extreme climate environments.

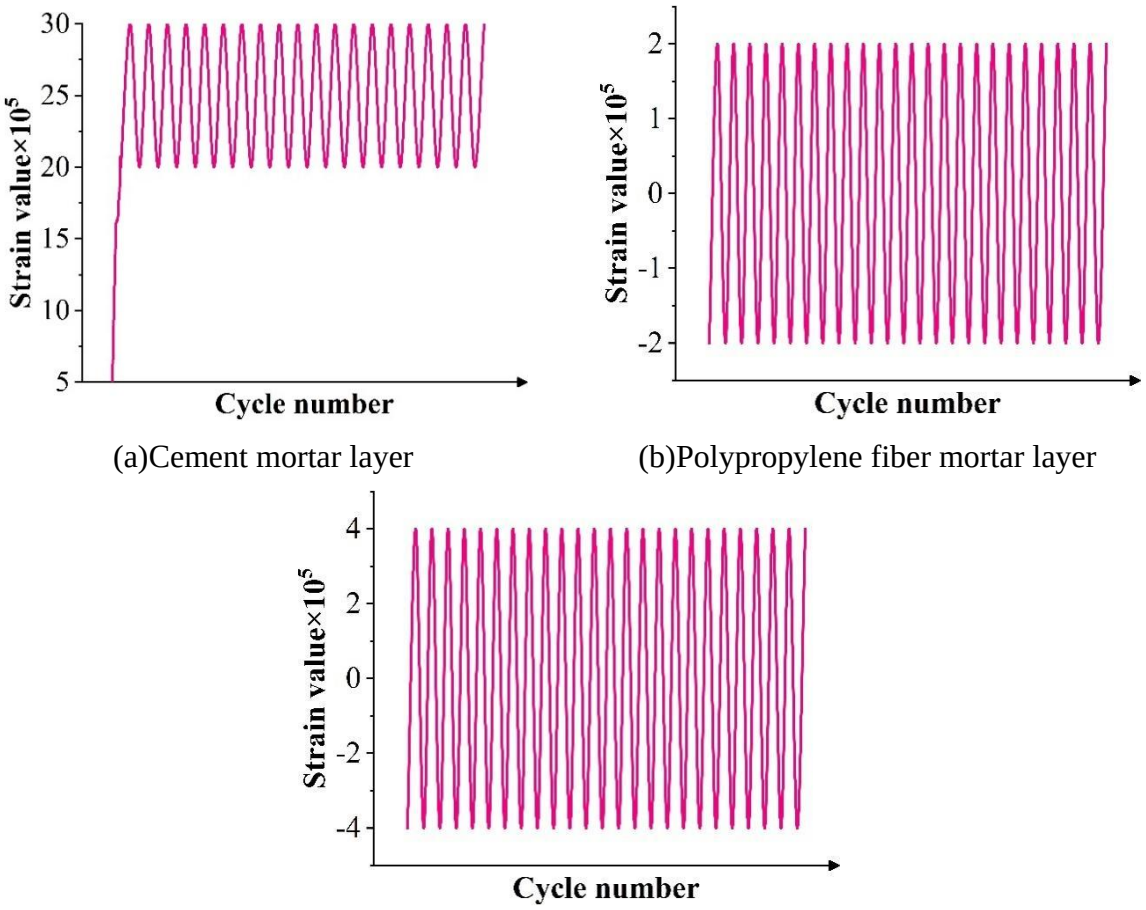

(a)Cement mortar layer (b)Polypropylene fiber mortar layer

(c)Polymer mortar layer

Figure 6: Strain simulation curve

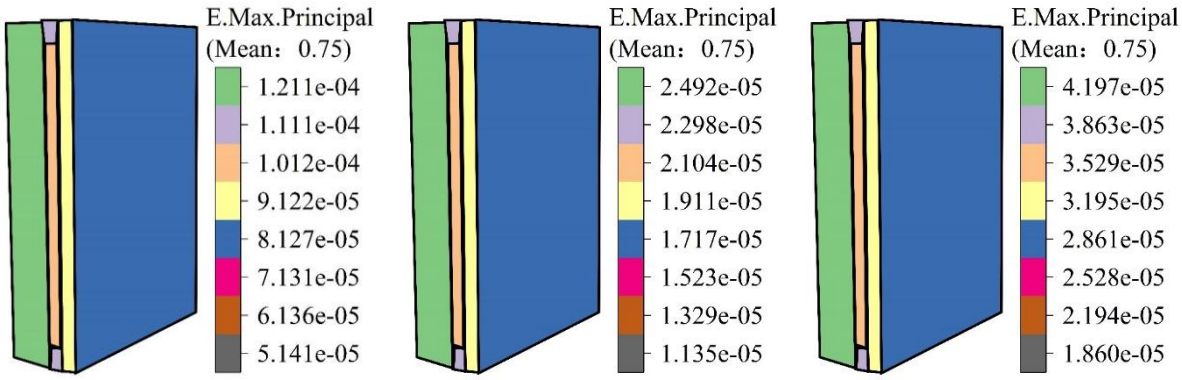

(a)Cement mortar layer (b)Polypropylene fiber mortar layer (c)Polymer mortar layer

Figure 7: Strain nephogram

4.4 Electrical-thermal-force analysis of materials

A 0.6mm-long model was split from one end of the finite element model of high-performance building materials, and a three-dimensional model of the specimen with dimensions of 800mm×80mm×0.8mm was created as the stress field analysis model. Under extreme climatic environment conditions, the electrothermal load information of the specimen was collected by

the polymer material electrothermal tester, and 6A, 10A and 14A currents were applied to the specimen to test the changes of thermal stresses on the surface ef the centerline of the specimen under the action of the three kinds of currents. The test results are shown in Fig. 8, where (a)~(c) denote the X, Y, and Z axes, respectively. In the case of increasing current intensity, the thermal stress of the specimen of high-performance building materials also increases with it, and the trend of thermal stress change of the specimen under different current intensities is similar, which can be seen in the extreme climatic environment conditions, this paper's specimen of high-performance building materials has obvious effect of hindering the thermal expansion, and the performance of thermal stress performance is stable.

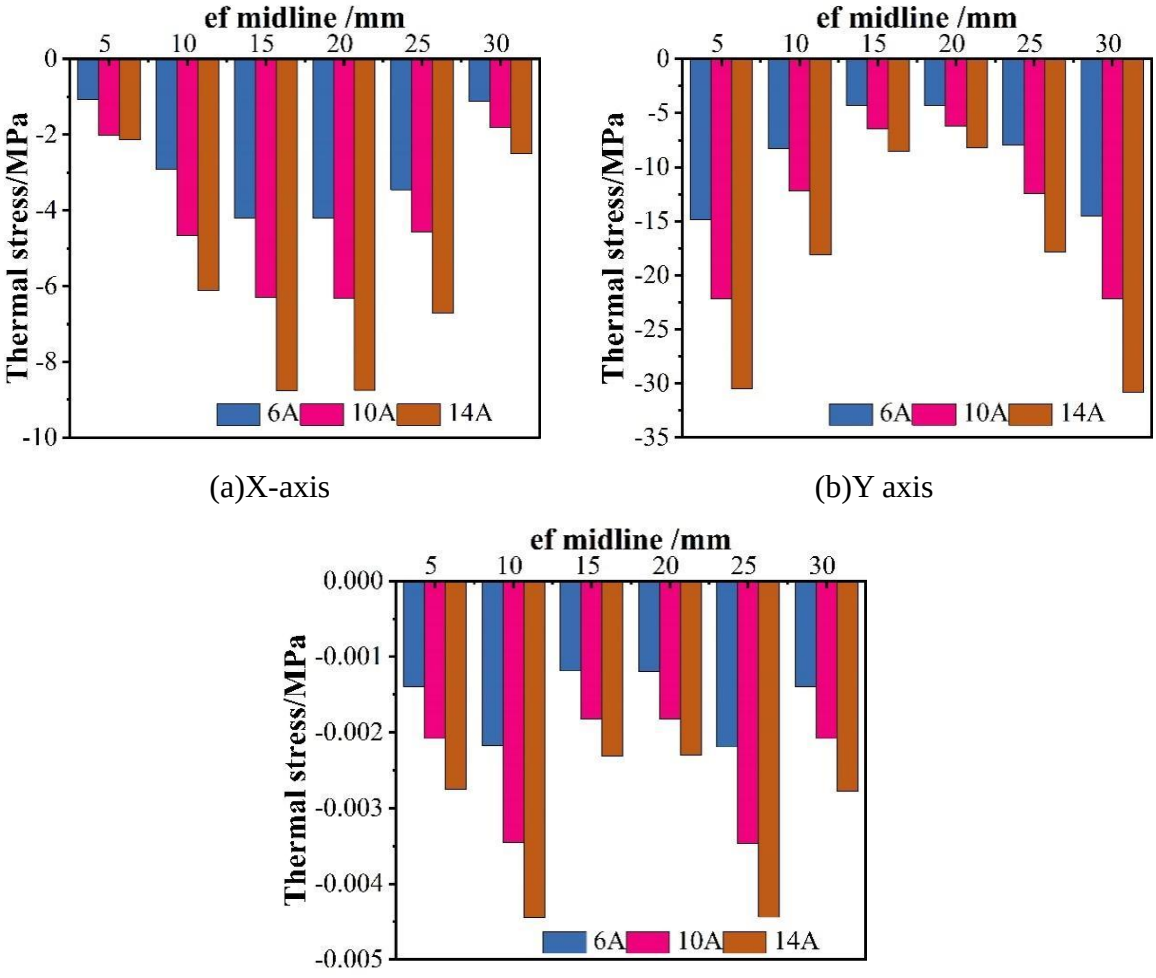

(a)X-axis (b)Y axis

(c)Z axis

Figure 8: Thermal stress variation of specimens under different currents

The change of current and thermal stress at X=20mm is presented separately and shown in Fig. 9. From Fig. 9, it can be seen more clearly that the thermal stress in the Z-axis direction is approximate to 0, and there is almost no fluctuation, and the change of thermal stress in the X and Y axes direction is more obvious, and the thermal stress and the current are in a kind of proportionality, which shows that the experimental specimen's X and Y axes direction is more significant to the obstruction of the thermal expansion, and the effect of the thermal stabilization is better.

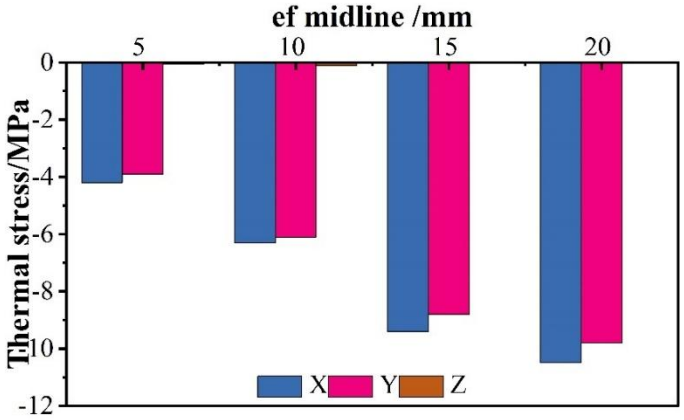

Figure 9: Current and thermal stress changes at X=15mm

4.5 Analysis of the effect of fiber volume content on thermal stability

Under extreme climatic conditions, in order to test the thermal stability of high-performance building materials specimens prepared with different fiber volume content, the stress-strain relationship of high-performance building materials specimens containing 5%, 10% and 15% of three different fiber volume content is examined, and the specimens are examined in a warming environment from -20℃ to 60℃, and the results are shown in Fig.10. In the same warming environment, the effect of increasing the fiber volume content of the specimen on the thermal performance of high-performance building materials can be reflected by the stress-strain relationship when reaching the same strain. In the same warming environment, the effect of increasing the fiber volume content of the specimen on the thermomechanical properties of high-performance building materials can be reflected by the stress-strain relationship, and when the same strain is reached, the higher the volume content of the fiber the higher the internal stress generated.

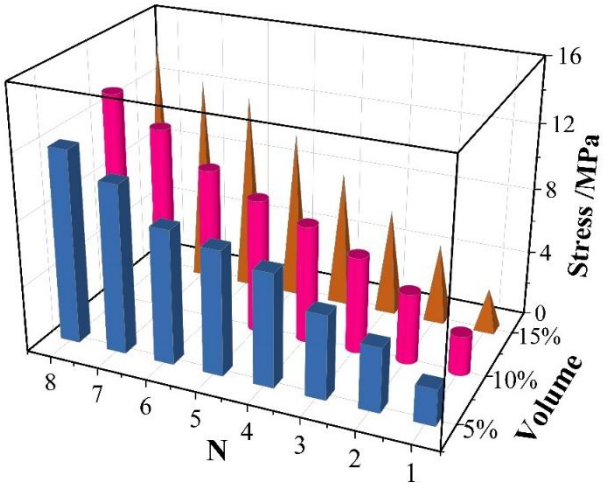

Figure 10: Stress-strain relationship test results

Continuing to test the relationship between the equivalent tensile modulus of specimens with different fiber volume contents and temperature in the temperature-raising environment, the test results are shown in Figure 11. Figure 11 can be derived from the same temperature conditions, the higher the fiber volume content of the specimen the higher the equivalent tensile modulus, with the increase in temperature of the equivalent tensile modulus of the specimen with different fiber volume content are slightly decreased, and the higher the content of the

specimen the more slight downward trend, it can be seen, high-performance building materials, the fiber volume content of the material directly affects its thermal stability, and the two are positively proportional to each other.

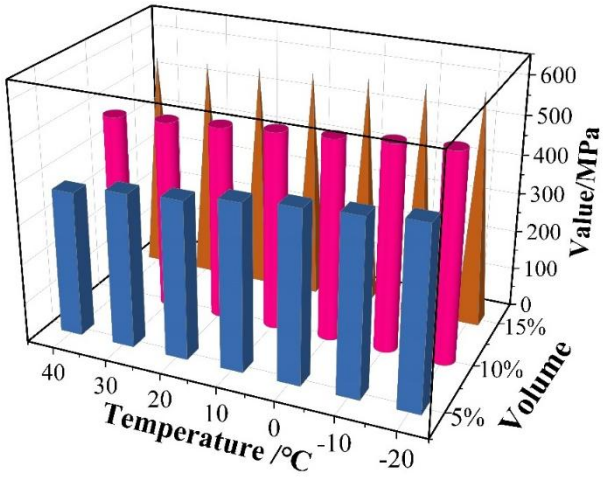

Figure 11: Relationship between equivalent tensile modulus and temperature change

5 Conclusion

This paper draws on the results of previous research, determines the raw materials for this study, and completes the preparation of high-performance building materials according to the corresponding preparation methods and processes. In order to present the research results more intuitively, ABAQU finite element simulation and analysis software is used to numerically simulate and analyze the thermal stress law of high-performance building materials in extreme climatic environments. In the extreme climate environment, with the increase of fiber volume content, the preparation of high-performance building materials thermal stress value shows a growing trend, from the initial 2.452MPa to 15.753MPa, clearly demonstrates the change rule of the thermal stress of high-performance building materials under extreme climatic conditions, and it has a guiding role in the field of materials development and innovation in the field of building engineering, and it promotes the rapid development of the building materials industry. The rapid development of the construction materials industry.

Funding

This work was supported by the 2026 Annual Key Scientific Research Project of Kaili University (Grant No. 2026ZD003) and the Modern Industrial College Project of Kaili University.

About the Author

Chen Jiao was born in Guizhou, P.R. China, in 1987. She obtained her master's degree in Sustainable Product Design from Singapore University of Technology and Design. She is currently an associate professor at the School of Architectural Engineering, Kaili University. Her main research directions are Architectural Design and Theory, Inheritance and Innovation of Traditional Architectural Culture, and Digital Low-Carbon Technology in Architecture.

jochen719@163.com

Zhi Zhuang was born in Jiangsu, P.R. China, in 1983. He obtained his PhD from Dalian University of Technology in China. He is currently an Associate Professor at the College of Architecture and Urban Planning, Tongji University. His main research directions include building environment simulation and optimization, adaptive building facades, building energy efficiency and smart operation and maintenance, building renewable energy technologies, and interdisciplinary exploration of the applications of performance-based design, artificial intelligence, and digital twin technology in architecture. 1008560@mymail.sutd.edu.sg

Jiankun Liang was born in in Hubei, P.R. China, in 1987. He obtained his PhD in Wood Science and Technology from Beijing Forestry University in China. He is currently an Associate Professor at the School of Architectural Engineering, Kaili University. His main research directions include the technological research and development and industrial application of wood-based composites and wood adhesives.joettenelleqs10@gmail.com

References

[1] Alsalman, A., Dang, C. N., & Hale, W. M. (2017). Development of ultra-high performance concrete with locally available materials. Construction and Building Materials, 133, 135-145.

[2] Wille, K., & Boisvert-Cotulio, C. (2015). Material efficiency in the design of ultra-high performance concrete. Construction and Building Materials, 86, 33-43.

[3] Lei, D. Y., Guo, L. P., Sun, W., Liu, J. P., & Miao, C. W. (2017). Study on properties of untreated FGD gypsum-based high-strength building materials. Construction and Building Materials, 153, 765-773.

[4] Jia, C., Chen, C., Mi, R., Li, T., Dai, J., Yang, Z., ... & Hu, L. (2019). Clear wood toward high-performance building materials. ACS nano, 13(9), 9993-10001.

[5] Zhang, P., Han, S., Golewski, G. L., & Wang, X. (2020). Nanoparticle-reinforced building materials with applications in civil engineering. Advances in Mechanical Engineering, 12(10), 1687814020965438.

[6] Chi, M. C., Chi, J. H., & Wu, C. H. (2018). Effect of GGBFS on compressive strength and durability of concrete. Advanced Materials Research, 1145, 22-26.

[7] Babalu, R., Anil, A., Sudarshan, K., & Amol, P. (2023). Compressive strength, flexural strength, and durability of high-volume fly ash concrete. Innovative Infrastructure Solutions, 8(5), 154.

[8] Gao, X., & Guo, Z. (2018). Mechanical stability, corrosion resistance of superhydrophobic steel and repairable durability of its slippery surface. Journal of colloid and interface science, 512, 239-248.

[9] Nordstrom, E. (2020). Durability of steel fibre reinforced shotcrete with regard to corrosion. In Shotcrete (pp. 213-217). CRC Press.

[10] Shen, J., Liang, J., Lin, X., Lin, H., Yu, J., & Yang, Z. (2020). Recent progress in polymer-based building materials. International Journal of Polymer Science, 2020(1), 8838160.

[11] Amran, M., Huang, S. S., Onaizi, A. M., Makul, N., Abdelgader, H. S., & Ozbakkaloglu, T. (2022). Recent trends in ultra-high performance concrete (UHPC): Current status, challenges, and future prospects. Construction and Building Materials, 352, 129029.

[12] Wu, N., Ji, T., Huang, P., Fu, T., Zheng, X., & Xu, Q. (2022). Use of sugar cane bagasse ash in ultra-high performance concrete (UHPC) as cement replacement. Construction and Building materials, 317, 125881.

[13] Burlayenko, V. N., Altenbach, H., Sadowski, T., Dimitrova, S. D., & Bhaskar, A. (2017). Modelling functionally graded materials in heat transfer and thermal stress analysis by means of graded finite elements. Applied Mathematical Modelling, 45, 422-438.

[14] Yi, R., Chen, C., Shi, C., Li, Y., Li, H., & Ma, Y. (2021). Research advances in residual thermal stress of ceramic/metal brazes. Ceramics International, 47(15), 20807-20820.

[15] Alvarado, J., Wei, C., Nordlund, D., Kroll, T., Sokaras, D., Tian, Y., ... & Doeff, M. M. (2020). Thermal stress-induced charge and structure heterogeneity in emerging cathode materials. Materials Today, 35, 87-98.

[16] Saffari, M., Piselli, C., De Gracia, A., Pisello, A. L., Cotana, F., & Cabeza, L. F. (2018). Thermal stress reduction in cool roof membranes using phase change materials (PCM). Energy and Buildings, 158, 1097-1105.

[17] Zhu, W., Zhang, Z. B., Yang, L., Zhou, Y. C., & Wei, Y. G. (2018). Spallation of thermal barrier coatings with real thermally grown oxide morphology under thermal stress. Materials & Design, 146, 180-193.

[18] Teguedi, M. C., Toussaint, E., Blaysat, B., Moreira, S., Liandrat, S., & Grédiac, M. (2017). Towards the local expansion and contraction measurement of asphalt exposed to freeze-thaw cycles. Construction and Building Materials, 154, 438-450.

[19] Nosov, S. V. (2018). Modeling the evolution of deformations and stresses in road-building materials based on rheological approach. Russian Journal of Building Construction and Architecture, (4), 61-72.

[20] Nizina, T. A., Selyaev, V. P., Nizin, D. R., Balykov, A. S., Korovkin, D. I., & Kanaeva, N. S. (2018, December). Application of fractal analysis methods in the study of deformation mechanisms and composite building materials fracture. In IOP Conference Series: Materials Science and Engineering (Vol. 456, No. 1, p. 012058). IOP Publishing.

[21] Shittu, S., Li, G., Zhao, X., Ma, X., Akhlaghi, Y. G., & Ayodele, E. (2019). High performance and thermal stress analysis of a segmented annular thermoelectric generator. Energy Conversion and Management, 184, 180-193.

[22] Yoo, D. Y., & Banthia, N. (2017). Mechanical and structural behaviors of ultra-high-performance fiber-reinforced concrete subjected to impact and blast. Construction and building materials, 149, 416-431.

[23] Amran, M., Murali, G., Makul, N., Tang, W. C., & Alluqmani, A. E. (2023). Sustainable development of eco-friendly ultra-high performance concrete (UHPC): Cost, carbon emission, and structural ductility. Construction and Building Materials, 398, 132477.

[24] Azmee, N. M., & Shafiq, N. (2018). Ultra-high performance concrete: From fundamental to applications. Case Studies in Construction Materials, 9, e00197.

[25] Wang, L., & Tang, S. (2022). High-Performance construction Materials: latest advances and Prospects. Buildings, 12(7), 928.

[26] Zhou, M., Lu, W., Song, J., & Lee, G. C. (2018). Application of ultra-high performance concrete in bridge engineering. Construction and Building Materials, 186, 1256-1267.

[27] Xue, J., Briseghella, B., Huang, F., Nuti, C., Tabatabai, H., & Chen, B. (2020). Review of ultra-high performance concrete and its application in bridge engineering. Construction and Building Materials, 260, 119844.

[28] Nahlik, M. J., Chester, M. V., Pincetl, S. S., Eisenman, D., Sivaraman, D., & English, P. (2017). Building thermal performance, extreme heat, and climate change. Journal of Infrastructure Systems, 23(3), 04016043.

[29] Kodur, V. K. R., Bhatt, P. P., Soroushian, P., & Arablouei, A. (2016). Temperature and stress development in ultra-high performance concrete during curing. Construction and Building Materials, 122, 63-71.

[30] Steinberg, E. P., Hussein, H. H., Walsh, K. K., & Sargand, S. M. (2016, July). Effect of extreme temperatures on the coefficient of thermal expansion for ultra-high performance concrete. In International Interactive Symposium on Ultra-High Performance Concrete (Vol. 1, No. 1). Iowa State University Digital Press.

[31] Ozawa, M., Tanibe, T., Kamata, R., Uchida, Y., Rokugo, K., & Parajuli, S. S. (2018). Behavior of ring-restrained high-performance concrete under extreme heating and development of screening test. Construction and Building Materials, 162, 215-228.

[32] Ramakrishnan, S., Wang, X., Sanjayan, J., & Wilson, J. (2017). Thermal performance of buildings integrated with phase change materials to reduce heat stress risks during extreme heatwave events. Applied energy, 194, 410-421.

[33] Van Hoa Cao & Gyu Hyun Go. (2024). A novel approach to stability analysis of random soil-rock mixture slopes using finite element method in ABAQUS. Natural Hazards,120(15),14381-14407.

[34] Siti Nor Asimah Hamid,Kannigah Thirunanasambantham,Zuhaila Ismail & Lim Yeou Jiann. (2025). Numerical Simulation of Heat Transfer in MHD Hybrid Blood Nanofluid Flow through a Bifurcated Stenosed Artery. Defect and Diffusion Forum,440,39-45.

[35] Sternberg Tobias,Marti Philippe & Jackson Andrew. (2025). Thermal convection in the internally heated sphere. Journal of Fluid Mechanics,1004(414),A14-A14.

[36] Ziheng Gu,Qiang Zang & Gaige Zheng. (2024). Near-unity nonreciprocal thermal radiation in biaxial van der Waals material-Weyl semimetal heterostructures. International Communications in Heat and Mass Transfer,153,107346-.